INTERNATIONAL JOURNAL FOR NUMERICAL METHODS IN ENGINEERING
Int. J. Numer. Meth. Engng 2002; **53**:225–242 (DOI: 10.1002/nme.399)

Extracting edge flux intensity functions for the Laplacian

Zohar Yosibash[1,*,†], Ricardo Actis[2] and Barna Szabó[2]

[1] *Mechanical Engineering Department, Pearlstone Center for Aeronautical Engineering Studies, Ben-Gurion University of the Negev, Beer-Sheva, Israel*
[2] *Mechanical Engineering Department, Washington University, St. Louis, MO 63130, U.S.A.*

This paper is dedicated to the memory of Professor Bernard Schiff

SUMMARY

The solution to the Laplace operator in three-dimensional domains in the vicinity of straight edges is presented as an asymptotic expansion involving eigenpairs with their coefficients called edge flux intensity functions (EFIFs). The eigenpairs are identical to their two-dimensional counterparts over a plane perpendicular to the edge. Extraction of EFIFs however, cannot be obtained in a straightforward manner over this two-dimensional plane. A method based on L^2 projection and Richardson extrapolation is presented for point-wise extraction of EFIFs from p-finite element solutions and illustrated by examples. A similar but more efficient method, based on 'energy projection', for extracting EFIFs is proposed. Copyright © 2001 John Wiley & Sons, Ltd.

KEY WORDS: singularities; generalized stress intensity functions; linear elasticity; p-version FEM

1. INTRODUCTION AND NOTATIONS

The solution of the Laplace problem in three-dimensional domains, in the vicinity of singularities, can be decomposed into three different forms, depending whether it is in the neighbourhood of an edge, a vertex or an intersection of the edge and the vertex. Mathematical details on the decomposition can be found e.g. in References [1–6] and the references therein. Herein we address edge singularities alone, and in particular, the extraction of the so-called edge flux intensity functions (EFIFs). *Only straight edges are considered* (for curved edges see Reference [2]) and the surfaces which intersect to form an edge are flat planes. A typical three-dimensional domain denoted by Ω, containing edge singularities, is shown in Figure 1. Edge singularities arise in the neighbourhood of the edges Λ_{ij} and away from the vertices.

We consider the equation:

$$\nabla^2_{3D} u = 0 \quad \text{in } \Omega \tag{1}$$

*Correspondence to: Zohar Yosibash, Mechanical Engineering Department, Ben-Gurion University, Beer-Sheva 84105, Israel
†E-mail: zohary@pversion.bgu.ac.il

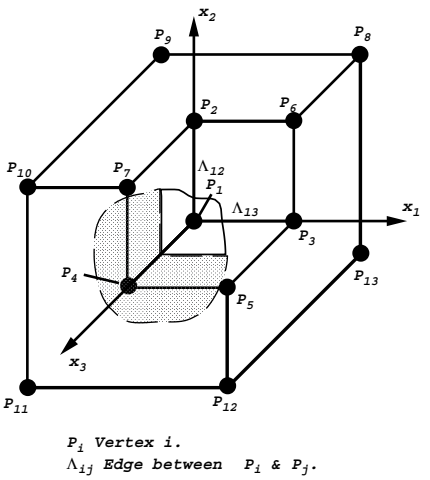

Figure 1. Typical 3-D edge singularities.

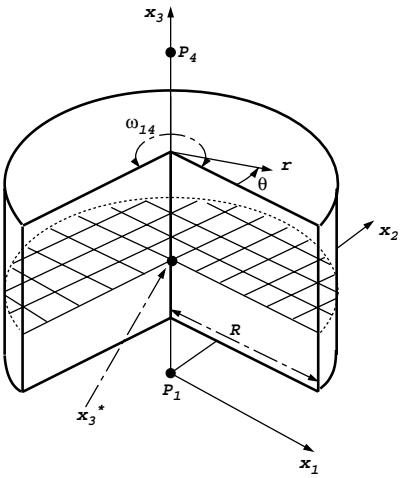

Figure 2. The edge sub-domain $\mathscr{E}(\Lambda_{14})$.

with the following boundary conditions:

$$B_1(u) = g_1 \quad \text{on } \Gamma_D \subset \partial\Omega \tag{2}$$

$$B_2(u) = g_2 \quad \text{on } \Gamma_N \subset \partial\Omega \tag{3}$$

where B_1 is the identity operator, B_2 is the outward normal derivative operator $\partial/\partial n$, g_i are given functions on the boundary and $\Gamma_D \cup \Gamma_N = \partial\Omega$. In the vicinity of edges of interest, homogeneous boundary conditions are assumed $B_i(u) \equiv 0$.

Consider one of the edges denoted by Λ_{14} connecting the vertices P_1 and P_4 and away from any of the vertices. We create a cylindrical sector sub-domain of radius $r = R$ with the edge Λ_{14} as its axis as shown in Figure 2. The solution in the neighbourhood of the edge can be decomposed as follows:

$$u(r,\theta,x_3) = \sum_{k=1}^{K} \sum_{\ell=0}^{L} a_{k\ell}(x_3) r^{\alpha_k} (\ln r)^{\ell} s_{k\ell}(\theta) + v(r,\theta,x_3) \tag{4}$$

where $L \geqslant 0$ is an integer which is zero except when α_k is an integer, $\alpha_{k+1} \geqslant \alpha_k$ are called edge eigenvalues, $a_{k\ell}(x_3)$ are called edge flux intensity functions EFIFs and are analytic in x_3 up to the vertices. The functions $s_{k\ell}(\theta)$ are analytic in θ, called edge eigenfunctions (the function $v(r,\theta,x_3)$ belongs in $H^q(\mathscr{E})$, the usual Sobolev space, where q can be as large as required and depends on K). We shall assume that α_k for $k \leqslant K$ are not integers, and that no 'crossing points' occur (see a detailed explanation in Reference [2]) therefore, (4) becomes

$$u(r,\theta,x_3) = \sum_{k=1}^{K} a_k(x_3) r^{\alpha_k} s_k(\theta) + v(r,\theta,x_3) \tag{5}$$

For (1), we may perform separation of variables in the neighbourhood of the edge singularity as shown in (5). Each function, (the nth for example, $r^{\alpha_n}s_n(\theta)$) is independent of x_3 and satisfies the Laplace equation over the plane (r,θ) which is perpendicular to the edge (the marked plane in Figure 2). *This is exactly a* 2-D *problem and the eigenpairs are identical to the* 2-D *eigenpairs* (for detailed mathematical analysis see Reference [6, Chapter 2.5]). Although for the Laplace operator the eigenpairs can be computed analytically, this is not the case for general scalar elliptic problems of the form

$$k_{11}(\theta)\frac{\partial^2 u}{\partial x_1^2} + 2k_{12}(\theta)\frac{\partial^2 u}{\partial x_1 \partial x_2} + k_{22}(\theta)\frac{\partial^2 u}{\partial x_2^2} = 0$$

where $k_{ij}(\theta)$ may be discontinuous in which case $s_k(\theta)$ are continuous piecewise analytic. For these cases numerical methods as the modified Steklov method described in Reference [7] should be used for determining the eigenpairs in the neighbourhood of edge singularities on a two-dimensional plane perpendicular to the edge (provided that in the x_3 direction the domain remains isotropic and the opening angle ω remains constant as well as the boundary conditions on the intersecting planes at the edge).

Section 2 provides in detail the asymptotic expansion of the solution to the Laplace equation in the neighbourhood of an edge singularity, followed by an analysis of a numerical method for extracting the pointwise values of the edge flux intensity functions (the L^2 projection method) in Section 3. An example problem with an exact solution for any polynomial edge flux intensity function is constructed in Section 4 against which numerical tests for demonstrating the mathematical analysis are reported. We thereafter introduce in Section 5 another numerical method for extracting the pointwise values of the edge flux intensity functions, based on the energy projection method. This method is more accurate and efficient compared with the method presented in Section 3. We conclude with a summary in Section 6.

2. THE ASYMPTOTIC EXPANSION IN THE NEIGHBOURHOOD OF AN EDGE SINGULARITY

Once the eigenpairs for the 2-D Laplacian are obtained, one may construct the full series expansion solution for the 3-D Laplacian. Let $r^{\alpha_n}s_n(\theta)$ be an eigenpair of the two-dimensional Laplacian (denoted by Δ_{2D}) over the x_1–x_2 plane perpendicular to an edge along the x_3-axis. Thus,

$$\Delta_{2D}[r^{\alpha_n}s_n(\theta)] = r^{\alpha_n-2}[\alpha_n^2 s_n(\theta) + s_n''(\theta)] = 0 \tag{6}$$

Let $a_n(x_3)$ be the edge flux intensity function associated with the eigenpair, it is clear that $a_n(x_3)r^{\alpha_n}s_n(\theta)$ does not satisfy the three-dimensional Laplacian, $\Delta_{3D} = \Delta_{2D} + \partial_3^2 = 0$, where $\partial_3^2 \stackrel{\text{def}}{=} \partial^2/\partial x_3^2$, unless $a_n(x_3)$ is a linear function in x_3:

$$\Delta_{3D}[a_n(x_3)r^{\alpha_n}s_n(\theta)] = \partial_3^2 a_n(x_3)r^{\alpha_n}s_n(\theta) \neq 0 \tag{7}$$

Augmenting the 2-D eigenfunction $a_n(x_3)r^{\alpha_n}s_n(\theta)$ by $(-1/4(\alpha_n+1))\partial_3^2 a_n(x_3)r^{\alpha_n+2}s_n(\theta)$ then substituting in the Laplace equation, one obtains

$$\Delta_{3D}\left[a_n(x_3)r^{\alpha_n}s_n(\theta)-\frac{1}{4(\alpha_n+1)}\partial_3^2 a_n(x_3)r^{\alpha_n+2}s_n(\theta)\right]=\frac{-1}{4(\alpha_n+1)}\partial_3^4 a_n(x_3)r^{\alpha_n+2}s_n(\theta)\neq 0 \quad (8)$$

The edge flux intensity function is a smooth function of the variable x_3, so that it may be approximated by polynomials. Examining (8), one may notice that if $a_n(x_3)$ is a polynomial of degree smaller or equal to three then the two terms inside the bracket are sufficient to form the solution to the 3-D Laplacian, associated with nth eigenpair. Otherwise, one needs to add a new term: $1/(32(\alpha_n+1)(\alpha_n+2))\partial_3^4 a_n(x_3)r^{\alpha_n+4}s_n(\theta)$, so that the residual becomes

$$\begin{aligned}\Delta_{3D}&\left[a_n(x_3)r^{\alpha_n}s_n(\theta)-\frac{1}{4(\alpha_n+1)}\partial_3^2 a_n(x_3)r^{\alpha_n+2}s_n(\theta)\right.\\&\left.+\frac{1}{32(\alpha_n+1)(\alpha_n+2)}\partial_3^4 a_n(x_3)r^{\alpha_n+4}s_n(\theta)\right]\\&=\frac{1}{32(\alpha_n+1)(\alpha_n+2)}\partial_3^6 a_n(x_3)r^{\alpha_n+4}s_n(\theta)\end{aligned} \quad (9)$$

The residual vanishes now if $a_n(x_3)$ is a polynomial of degree less than or equal to five. We may proceed in a similar fashion, and obtain the following function $S_n(r,\theta,x_3)$ associated with the 2-D function $r^{\alpha_n}s_n(\theta)$:

$$S_n(r,\theta,x_3)=r^{\alpha_n}s_n(\theta)\sum_{i=0}^{\infty}\partial_3^{2i}a_n(x_3)r^{2i}\frac{(-1/4)^i}{\prod_{j=1}^{i}j(\alpha_n+j)} \quad (10)$$

This function satisfies identically the 3-D Laplace equation: $\Delta_{3D}S_n\equiv 0$. If series (10) is truncated at the Nth term the remainder which does not satisfy the 3-D Laplace equation is

$$\partial_3^{2N+2}a_n(x_3)r^{\alpha_n+2N}s_n(\theta)\frac{(-1/4)^N}{\prod_{j=1}^{N}j(\alpha_n+j)} \quad (11)$$

Thus the three-dimensional edge singular solution (5) can be also represented as

$$\begin{aligned}u(r,\theta,x_3)&=\sum_{i=k}^{K}S_k(r,\theta,x_3)+v(r,\theta,x_3)\\&=\sum_{k=1}^{K}a_k(x_3)r^{\alpha_k}s_k(\theta)+c_{k1}\partial_3^2 a_k(x_3)r^{\alpha_k+2}s_k(\theta)\\&\quad+c_{k2}\partial_3^4 a_k(x_3)r^{\alpha_k+4}s_k(\theta)+\cdots+v(r,\theta,x_3)\end{aligned} \quad (12)$$

where c_{ij} are given constants. In Appendix A it is proven that the above series expansion can be brought to the classical representation of the solution in terms of Bessel functions. Having

computed the 3-D expansion of the solution in terms of eigenpairs, one may proceed to the computation of the edge flux intensity functions $a_n(x_3)$.

Remark 1
The eigenfunctions $s_n(\theta)$ are orthogonal in the sense that

$$\int_{\theta=0}^{\omega_{ij}} s_n s_m \, \mathrm{d}\theta = 0 \quad \text{for } m \neq n$$

i.e., any two terms in the 2-D singular series expansion are orthogonal to each other. This property is exploited in methods as the contour integral method (see e.g. Reference [8]) for extracting efficiently the flux intensity factors in 2-D domains. However, in 3-D domains, since higher order terms $(r^{\alpha_n+2}, r^{\alpha_n+4}, \ldots)$ in expansion (11) consist of the same functions $s_n(\theta)$ as the other lower order terms, then terms in the series expansion are no longer orthogonal. This impose difficulties in implementing the contour integral method for 3-D domains, and remedies must be sought.

3. EXTRACTING POINTWISE VALUES OF THE EFIFs BY THE L^2 PROJECTION METHOD

Let us define the space spanned by the 2-D Laplacian eigenpairs by $\mathfrak{S}_{2D}$:

$$\mathfrak{S}_{2D} \stackrel{\text{def}}{=} \{u_n(r,\theta) = r^{\alpha_n} s_n(\theta) | \Delta_{2D} u_n = 0, \; B_i(u) = 0, \; i = 1,2 \text{ on the planes intersecting at the edge}\} \tag{13}$$

We wish to obtain a L^2 projection of the solution of the 3-D Laplace equation in the vicinity of an edge in the plane perpendicular to the edge, intersecting it at a given point x_3^*, into a subspace $\mathfrak{S}_{2D}^N \subset \mathfrak{S}_{2D}$. This subspace $\mathfrak{S}_{2D}^N$ is spanned by the first N eigenpairs. Therefore, each $u^N \in \mathfrak{S}_{2D}^N$ is a linear combination of functions in $\mathfrak{S}_{2D}^N$:

$$u^N = \sum_{i=1}^{N} b_i(x_3^*) r^{\alpha_i} s_i(\theta) \tag{14}$$

The projection operation is aimed at finding these $b_i(x_3^*)$ so that the error $u(x_3^*) - u^N(x_3^*)$ is orthogonal to the space $\mathfrak{S}_{2D}^N$ at the point x_3^*. i.e. it has to be orthogonal to any $v^N(x_3^*) \in \mathfrak{S}_{2D}^N$:

$$\int_r \int_\theta (u - u^N) v^N |_{x_3 = x_3^*} r \, \mathrm{d}r \, \mathrm{d}\theta = 0 \quad \forall v^N(x_3^*) \in \mathfrak{S}_{2D}^N \tag{15}$$

The above can be rephrased in the form

Find $u^N(x_3^*) \in \mathfrak{S}_{2D}^N$ so that

$$\int_r \int_\theta u v^N |_{x_3 = x_3^*} r \, \mathrm{d}r \, \mathrm{d}\theta = \int_r \int_\theta u^N v^N |_{x_3 = x_3^*} r \, \mathrm{d}r \, \mathrm{d}\theta \quad \forall v^N(x_3^*) \in \mathfrak{S}_{2D}^N \tag{16}$$

v^N being in $\mathfrak{S}_{2D}^N$ allows the representation

$$v^N(x_3^*) = \sum_{i=1}^{N} d_i(x_3^*) r^{\alpha_i} s_i(\theta) \tag{17}$$

Let us first concentrate on the right-hand side (RHS) of (16), which after substitution of (14) and (17) becomes

$$\begin{aligned}\mathrm{RHS} = {} & b_1(x_3^*)d_1(x_3^*)\int_r\int_\theta r^{2\alpha_1+1}s_1^2(\theta)\,\mathrm{d}r\,\mathrm{d}\theta \\ & + b_1(x_3^*)d_2(x_3^*)\int_r\int_\theta r^{\alpha_1+\alpha_2+1}s_1(\theta)s_2(\theta)\,\mathrm{d}r\,\mathrm{d}\theta \\ & + b_2(x_3^*)d_1(x_3^*)\int_r\int_\theta r^{\alpha_1+\alpha_2+1}s_1(\theta)s_2(\theta)\,\mathrm{d}r\,\mathrm{d}\theta \\ & + b_2(x_3^*)d_2(x_3^*)\int_r\int_\theta r^{2\alpha_2+1}s_2^2(\theta)\,\mathrm{d}r\,\mathrm{d}\theta + \cdots \end{aligned} \tag{18}$$

The eigenfunctions of the Laplace equation with homogeneous boundary conditions in the vicinity of the edge are orthogonal (see Remark 1), so that after integrating (18) in the radial direction from $r=0$ to R becomes

$$\mathrm{RHS} = \sum_{i=1}^{N} b_i(x_3^*)d_i(x_3^*)\frac{R^{2\alpha_i+2}}{2\alpha_i+2}\int_\theta s_i^2(\theta)\,\mathrm{d}\theta \tag{19}$$

Let us now consider the LHS. Although u is given (and may thereafter be replaced by u_{FE} if not known), we will use its full expansion given by (12). Substituting (12) and (17) in the LHS of (16) one obtains

$$\begin{aligned}\mathrm{LHS} = {} & a_1(x_3^*)d_1(x_3^*)\int_r\int_\theta r^{2\alpha_1+1}s_1^2(\theta)\,\mathrm{d}r\,\mathrm{d}\theta \\ & + c_{11}(\partial_3^2 a_1(x_3^*))d_1(x_3^*)\int_r\int_\theta r^{2\alpha_1+3}s_1^2(\theta)\,\mathrm{d}r\,\mathrm{d}\theta \\ & + c_{12}(\partial_3^4 a_1(x_3^*))d_1(x_3^*)\int_r\int_\theta r^{2\alpha_1+5}s_1^2(\theta)\,\mathrm{d}r\,\mathrm{d}\theta \\ & + \cdots \\ & + a_2(x_3^*)d_2(x_3^*)\int_r\int_\theta r^{2\alpha_2+1}s_2^2(\theta)\,\mathrm{d}r\,\mathrm{d}\theta \\ & + c_{21}(\partial_3^2 a_2(x_3^*))d_2(x_3^*)\int_r\int_\theta r^{2\alpha_2+3}s_2^2(\theta)\,\mathrm{d}r\,\mathrm{d}\theta \\ & + c_{22}(\partial_3^4 a_2(x_3^*))d_2(x_3^*)\int_r\int_\theta r^{2\alpha_2+5}s_2^2(\theta)\,\mathrm{d}r\,\mathrm{d}\theta \\ & + \cdots \\ = {} & \sum_{i=1}^{\infty}\int_\theta s_i^2(\theta)\,\mathrm{d}\theta\frac{R^{2\alpha_i+2}}{2\alpha_i+2}\left\{a_i(x_3^*)d_i(x_3^*) + R^2\frac{c_{i1}(\alpha_i+1)}{\alpha_i+2}(\partial_3^2 a_i(x_3^*))d_i(x_3^*)\right. \\ & \left. + R^4\frac{c_{i2}(\alpha_i+1)}{\alpha_i+3}(\partial_3^4 a_i(x_3^*))d_i(x_3^*) + R^6\frac{c_{i3}(\alpha_i+1)}{\alpha_i+4}(\partial_3^6 a_i(x_3^*))d_i(x_3^*) + \cdots\right\} \end{aligned} \tag{20}$$

Since RHS has to be equal to the LHS for every $d_i(x_3^*)$, by substituting (19) and (20) in (16) one obtains a set of equations for the coefficients $b_i(x_3^*)$:

$$b_i(x_3^*) = a_i(x_3^*) + R^2 \frac{c_{i1}(\alpha_i + 1)}{\alpha_i + 2}(\partial_3^2 a_i(x_3^*)) + R^4 \frac{c_{i2}(\alpha_i + 1)}{\alpha_i + 3}(\partial_3^4 a_i(x_3^*)) + \mathcal{O}(R^6) \tag{21}$$

Examining (21) it is seen that $b_i(x_3^*)$'s are not equal to $a_i(x_3^*)$ as desired, but include additional terms. These are associated with $R^{2n}\partial_{x_3}^{2n} a_i(x_3^*)$, $n = 1, 2, \ldots$. To eliminate these higher order terms, one needs to compute the $b_i(x_3^*)$'s at decreasing values of $R < 1$, followed by Richardson's extrapolation as in Reference [9]. The accuracy of the method will be demonstrated by the numerical examples. It is clear that when the loading is constant or depends linearly on x_3, then $a_i(x_3)$ are at most linear in x_3, so that (21) simplifies to $b_i(x_3^*) = a_i(x_3^*)$ and the extracted values are independent of R. This will be demonstrated by numerical examples in Section 4.

3.1. The L^2 projection method—numerical implementation

Since the exact solution u in (16) is unknown, we use instead an approximation, namely the finite element solution u_{FE}. This approximation introduces the second source of numerical error (the first source is due to the finite R and the need of Richardson's extrapolation). Any function $u^N \in \mathfrak{S}_{2\mathrm{D}}^N$ may be represented as

$$u^N = (b_1 \;\; b_2 \;\; \cdots \;\; b_N) \begin{Bmatrix} r^{\alpha_1} s_1(\theta) \\ r^{\alpha_2} s_2(\theta) \\ . \\ . \\ r^{\alpha_N} s_N(\theta) \end{Bmatrix} \stackrel{\mathrm{def}}{=} \mathbf{b}^T \begin{Bmatrix} r^{\alpha_1} s_1(\theta) \\ r^{\alpha_2} s_2(\theta) \\ . \\ . \\ r^{\alpha_N} s_N(\theta) \end{Bmatrix} \tag{22}$$

and similarly,

$$v^N = \{r^{\alpha_1} s_1(\theta) \;\; r^{\alpha_2} s_2(\theta) \;\; \cdots \;\; r^{\alpha_N} s_N(\theta)\}\mathbf{d} \tag{23}$$

Substituting (22) and (23) in (16), with u replaced by u_{FE}, one obtains the following system:
Find $\mathbf{b}$ such that

$$\int_{r=0}^{R} \int_{\theta=0}^{\omega_{14}} u_{\mathrm{FE}} \{r^{\alpha_1} s_1(\theta) \;\; r^{\alpha_2} s_2(\theta) \;\; \cdots \;\; r^{\alpha_N} s_N(\theta)\}\mathbf{d}(x_3^*) r \, \mathrm{d}r \, \mathrm{d}\theta$$

$$= \int_{r=0}^{R} \int_{\theta=0}^{\omega_{14}} \mathbf{b}^T(x_3^*) \begin{Bmatrix} r^{\alpha_1} s_1(\theta) \\ r^{\alpha_2} s_2(\theta) \\ . \\ . \\ r^{\alpha_N} s_N(\theta) \end{Bmatrix} \{r^{\alpha_1} s_1(\theta) \;\; r^{\alpha_2} s_2(\theta) \;\; \cdots \;\; r^{\alpha_N} s_N(\theta)\}\mathbf{d}(x_3^*) r \, \mathrm{d}r \, \mathrm{d}\theta \quad \forall \mathbf{d}(x_3^*) \tag{24}$$

(24) can be brought to a matrix representation:

$$\mathbf{L}^T\mathbf{d}(x_3^*)=\mathbf{b}^T(x_3^*)[S]\mathbf{d}(x_3^*)\quad\forall\mathbf{d}(x_3^*) \tag{25}$$

where

$$S_{ij}=\int_{r=0}^{R}\int_{\theta=0}^{\omega_{14}} r^{\alpha_i+\alpha_j}s_i(\theta)s_j(\theta)r\,\mathrm{d}r\,\mathrm{d}\theta=\frac{R^{\alpha_i+\alpha_j+2}}{\alpha_i+\alpha_j+2}\int_{\theta=0}^{\omega_{14}} s_i(\theta)s_j(\theta)\,\mathrm{d}\theta \tag{26}$$

and in view of Remark 1:

$$S_{ij}=\begin{cases}\dfrac{R^{2\alpha_i+2}}{2\alpha_i+2}\displaystyle\int_{\theta=0}^{\omega_{14}} s_i^2(\theta)\,\mathrm{d}\theta, & i=j\\ 0, & i\neq j\end{cases} \tag{27}$$

The elements of the vector $\mathbf{L}$ have to be computed numerically because u_{FE} is extracted from the finite element solution:

$$L_i=\int_{r=0}^{R}\int_{\theta=0}^{\omega_{14}} u_{\mathrm{FE}}(r,\theta,x_3^*)r^{\alpha_i+1}s_i(\theta)\,\mathrm{d}r\,\mathrm{d}\theta \tag{28}$$

Since (25) has to hold for any $\mathbf{d}(x_3^*)$, then it is equivalent to

$$\mathbf{L}^T=\mathbf{b}^T(x_3^*)[S] \tag{29}$$

Substituting (27) and (28) in (29), and noticing that $[S]$ is a diagonal matrix, one obtains explicit equations for the required elements of the vector $\mathbf{b}$:

$$b_i(x_3^*)=L_i\Big/\left(\frac{R^{2\alpha_i+2}}{2\alpha_i+2}\int_{\theta=0}^{\omega_{14}} s_i^2(\theta)\,\mathrm{d}\theta\right) \tag{30}$$

Notice that the numerical error caused by the replacement of u with u_{FE} is reflected in L_i, however this error is smaller than the pointwise error. This is due to the cancelations in the integration.

Because the accuracy of the finite element solution u_{FE} in the elements near the singularity is low, the following strategy is adopted for the computation of the b_i's. Instead of integrating on a sector from $r=0$ to R, the integration in (26) and (28) is performed over a circular ring, $r=0.9R$ to R. Thus instead of using (30) for the computation of the b_i's, we use the following:

$$b_i(x_3^*)=\int_{0.9R}^{R}\int_{\theta=0}^{\omega_{14}} u_{\mathrm{FE}}(r,\theta,x_3^*)r^{\alpha_i+1}s_i(\theta)\,\mathrm{d}r\,\mathrm{d}\theta\Big/\left(\frac{(1-0.9^{2\alpha_i+2})R^{2\alpha_i+2}}{2\alpha_i+2}\int_{\theta=0}^{\omega_{14}} s_i^2(\theta)\,\mathrm{d}\theta\right) \tag{31}$$

The numerical error in u_{FE} can be controlled by an adaptive finite element solution using p-extension.

The vector $\mathbf{b}(x_3^*)$ has to be extracted with a tight control of the numerical error using (30) at various R's of decreasing order. Then Richardson's extrapolating method has to be applied for estimating the exact value at $R\to 0$. The overall algorithm is illustrated in the

next subsection on the basis of a model problem constructed such that the exact solution is known.

4. AN EXAMPLE PROBLEM AND NUMERICAL EXPERIMENTATION

In order to test the accuracy of any numerical algorithm for extracting edge flux intensity functions one needs to generate example problems having analytical solutions. These example problems must allow a general solution in terms of EFIFs, i.e. they have to represent constant, linear, quadratic, etc. variation of the EFIFs along an edge of interest. In view of the analytical functional representation of the solution in the neighbourhood of the singular edge (12) we may construct a family of example problems as follows. Consider a domain shaped as a sector of a cylinder as shown in Figure 3. The edge of interest is OD aligned along the x_3 axis. On the faces ODEA and ODCB we impose flux free boundary conditions: $\mathbf{q}_n = 0$. On the cylindrical boundary AECB, at which $r = 2$, Dirichlet boundary conditions are imposed according to the series (12):

$$u(r=2,\theta,x_3) = (a_{11} + a_{12}x_3 + a_{13}x_3^2)2^{\alpha_1}\cos(\alpha_1\theta) - a_{13}\frac{1}{2(\alpha_1+1)}2^{\alpha_1+2}\cos(\alpha_1\theta)$$
$$+ (a_{21} + a_{22}x_3 + a_{23}x_3^2)2^{\alpha_2}\cos(\alpha_2\theta) - a_{13}\frac{1}{2(\alpha_2+1)}2^{\alpha_2+2}\cos(\alpha_2\theta) \quad (32)$$

where $\alpha_i = i\pi/\omega$. Note that the flux free boundary conditions on ODEA and ODCB are identically satisfied by (32). On the face $x_3 = 0$ of the domain we impose the Dirichlet boundary conditions:

$$u(r,\theta,x_3=0) = a_{11}r^{\alpha_1}\cos(\alpha_1\theta) - a_{13}\frac{1}{2(\alpha_1+1)}r^{\alpha_1+2}\cos(\alpha_1\theta)$$
$$+ a_{21}r^{\alpha_2}\cos(\alpha_2\theta) - a_{13}\frac{1}{2(\alpha_2+1)}r^{\alpha_2+2}\cos(\alpha_2\theta) \quad (33)$$

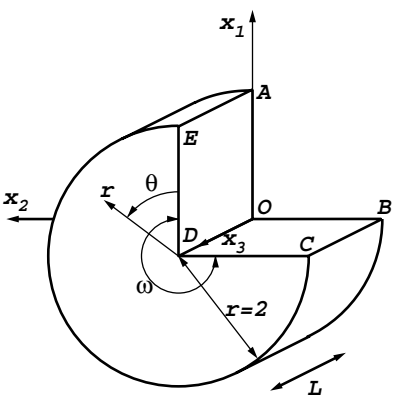

Figure 3. 3-D domain for example problems for EFIFs.

On the boundary of the domain $x_3 = L$ we may impose Dirichlet boundary conditions according to (32), i.e.:

$$u(r,\theta,x_3=L) = (a_{11} + a_{12}L + a_{13}L^2)r^{\alpha_1}\cos(\alpha_1\theta) - a_{13}\frac{1}{2(\alpha_1+1)}r^{\alpha_1+2}\cos(\alpha_1\theta)$$
$$+ (a_{21} + a_{22}L + a_{23}L^2)r^{\alpha_2}\cos(\alpha_2\theta) - a_{13}\frac{1}{2(\alpha_2+1)}r^{\alpha_2+2}\cos(\alpha_2\theta) \quad (34)$$

or we may impose flux free boundary conditions which will excite vertex singularities. Choosing $a_{11} = 1$, and $a_{21} = 2$ for example, and letting the other $a_{ij} = 0$, the EFIFs will be constant, and the numerical algorithm for extracting EFIFs should recover a_{11} and a_{21}. Choosing in addition $a_{12} = 3$, for example, we generate a model problem for which the EFIF $a_1(x_3)$ has a linear variation along the edge. If we wish to have parabolic variation of both $a_1(x_3)$ and $a_2(x_3)$, we may chose in addition $a_{22} = 4$, $a_{13} = 5$ and $a_{23} = 6$. We may proceed in a similar manner and obtain higher polynomial variation of the EFIFs, or add more terms thus having more EFIFs. The numerical computation of EFIFs should recover these values of a_{ij} if the algorithm is accurate.

It is important to emphasize that in the neighbourhood of O and D vertex singularities may arise, and therefore the EFIFs should be extracted away from these vertices. As the 'length' of the domain is increased (L taken larger), the vertex influence decreases. In the finite element simulation, a graded mesh towards O and D is recommended, and the EFIFs might be extracted in the mid-portion of the edge OD.

4.1. Computing EFIFs using L^2 projection method—an example problem

Consider the domain presented in Figure 3 with the following boundary conditions: on ODEA and ODCB: $\mathbf{q}_n = 0$. On the cylindrical boundary ($r = 2$), and on $x_3 = 0$ and $x_3 = L = 2$ Dirichlet BCs. are imposed according to

$$u = (a_{11} + a_{12}x_3 + a_{13}x_3^2)r^{\alpha_1}\cos(\alpha_1\theta) - a_{13}\frac{1}{2(\alpha_1+1)}r^{\alpha_1+2}\cos(\alpha_1\theta)$$
$$+ (a_{21} + a_{22}x_3 + a_{23}x_3^2)r^{\alpha_2}\cos(\alpha_2\theta) - a_{13}\frac{1}{2(\alpha_2+1)}r^{\alpha_2+2}\cos(\alpha_2\theta), \quad \alpha_i = i\pi/\omega$$

A finite element mesh containing 12 solid elements (hexahedra and pentahedra) is constructed with three refined layers in the neighbourhood of the singular edge (radius of smallest element is $0.15^3 \times 2$). The finite element mesh with the zoomed area in the neighbourhood of the singular edge is shown in Figure 4. We perform on the given mesh two analysis. In the first, we chose $a_{i1} = 1$, $a_{i2} = 0.5$, and $a_{i3} = 0$ $i = 1, 2$, thus the first two EFIFs are linear in x_3:

$$a_1(x_3) = 1 + 0.5x_3, \quad a_2(x_3) = 1 + 0.5x_3$$

According to the mathematical analysis the extracted EFIFs based on L^2 projection should be independent of the radius ($\partial_3^{2k} a_i(x_3) = 0$ $\forall k = 1, 2, \ldots$) and accurate.

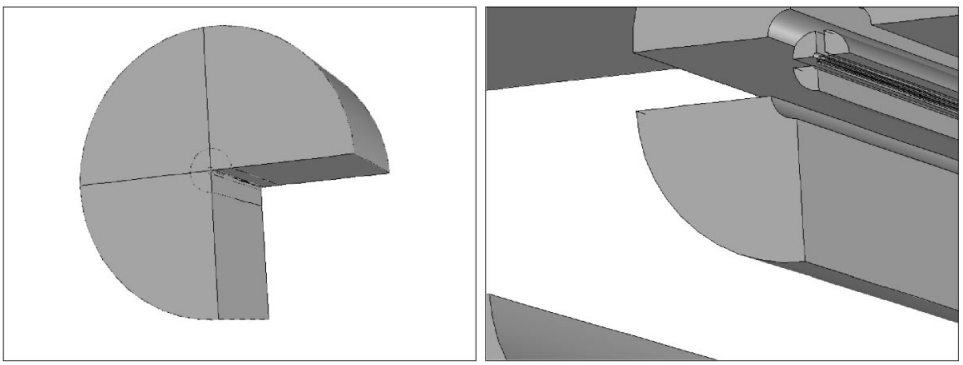

Figure 4. 3-D p-FEM (12 elements).

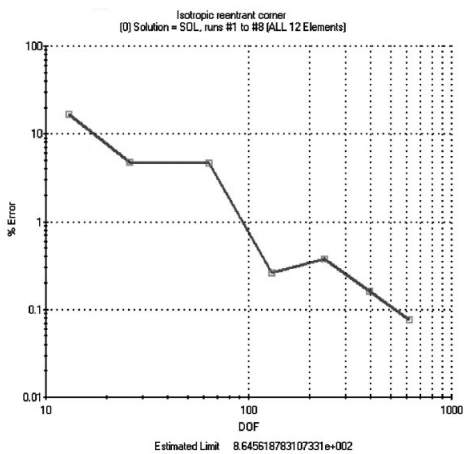

Figure 5. Convergence of the error in energy-norm for second analysis.

In the second analysis we chose $a_{i1}=1$, $a_{i2}=0.5$, and $a_{i3}=2$ $i=1,2$, thus the first two EFIFs are parabolic in respect to x_3:

$$a_1(x_3)=1+0.5x_3+2x_3^2, \quad a_2(x_3)=1+0.5x_3+2x_3^2$$

For this case one should clearly see a strong dependence of the extracted EFIFs on the radius of the integration area R, and that the extracted values converge to the exact solution as $R\to 0$.

Since the finite element solution is used in the numerical procedure described in Section 3.1, the error of approximation must be determined before computing the EFIFs. Figure 5 shows the estimated relative error in energy norm as a function of the number of degrees of freedom (DOF) for the second analysis. The degrees of freedom were systematically increased by p-extension on the fixed mesh shown in Figure 4.

Table I. Values of b_1 and b_2 for first analysis where $a_1(x_3) = 1 + 0.5x_3$, $a_2(x_3) = 1 + 0.5x_3$.

	$R = 1$	$R = 0.2$	$R = 0.1$	$R = 0.01$	a_i^{EX}
$b_1(x_3^* = 0.5)$	1.250	1.250	1.250	1.250	1.250
$b_1(x_3^* = 1.0)$	1.500	1.500	1.500	1.499	1.500
$b_2(x_3^* = 0.5)$	1.250	1.250	1.250	1.250	1.250
$b_2(x_3^* = 1.0)$	1.500	1.500	1.500	1.500	1.500

Table II. Values of b_1 and b_2 for second analysis where $a_1(x_3) = 1 + 0.5x_3 + 2x_3^2$, $a_2(x_3) = 1 + 0.5x_3 + 2x_3^2$.

	$R = 1$	$R = 0.2$	$R = 0.1$	$R = 0.01$	a_i^{EX}
$b_1(x_3^* = 0.5)$	1.206	1.729	1.745	1.750	1.750
$b_1(x_3^* = 1.0)$	2.955	3.476	3.492	3.499	3.500
$b_2(x_3^* = 0.5)$	1.360	1.735	1.747	1.750	1.750
$b_2(x_3^* = 1.0)$	3.109	3.483	3.494	3.499	3.500

Table III. $b_1(x_3^* = 0.5)$ for various values of R, $p = 8$, and the Richardson's extrapolated values as $R \to 0$.

R	$b_1(x_3^* = 0.5) \stackrel{\mathrm{def}}{=} b_1^{(0)}$	$b_1^{(1)}$	$b_1^{(2)}$
1.0	1.206		
		1.7477	
0.75	1.443		1.7494
		1.7490	
0.5	1.613		

The first two non-zero EFIFs extracted using different radii at $x_3^* = 1$ and 0.5, for the first analysis are summarized in Table I.

As predicted by the mathematical analysis, the extracted EFIFs are independent of the radius R (outer radius of integration for the L^2 projection).

For the second analysis, with $a_{i3} \neq 0$, the extracted EFIFs are R-dependent. We summarize in Table II the first two non-zero EFIFs extracted using different radii at $x_3^* = 1$ and 0.5. It is seen that the extracted EFIFs in this case have a strong dependency on the radius of the domain on which the extraction is performed, and indeed as $R \to 0$, the extracted value approaches the exact EFIFs. However, based on the mathematical analysis, it is possible to use Richardson's extrapolation starting with the value of R and extrapolate to $R = 0$. As an example, let us extract the values of b_1 and b_2 at $R = 1, 0.75, 0.5$, where these are known to be wrong. Using Richardson's extrapolation, with the residual error behaving as R^2 (this is known from (21)), we show that very close approximation for a_i can be obtained. For example let us chose the point $x_3^* = 0.5$ and extract $b_1(x_3^* = 0.5)$. The second column in Table III represents

Table IV. $b_2(x_3^* = 0.5)$ for various values of R, $p = 8$, and the Richardson's extrapolated values as $R \to 0$.

R	$b_2(x_3^* = 0.5) \stackrel{\text{def}}{=} b_2^{(0)}$	$b_2^{(1)}$	$b_2^{(2)}$
1.0	1.360		
		1.7485	
0.75	1.530		1.7499
		1.7496	
0.5	1.652		

the extracted values from the FE solution. One observes that although the extracted values at large R are far from the exact values, the extrapolated value is very close to the exact value (0.03 per cent relative error).

The same procedure is applied to $b_2(x_3^* = 0.5)$ as shown in Table IV. The extrapolated value of $b_2(x_3^* = 0.5)$ is again very close to the exact solution.

5. THE ENERGY PROJECTION METHOD

Similarly to the L^2 projection method, the energy projection method projects u into $\mathfrak{S}_{2D}^N$. The difference is the projection method which is based on the gradient of the function, i.e. we wish to find a member in $\mathfrak{S}_{2D}^N$ which is as close as possible to the function u so that the error between their gradients is minimized:

Find $u^N(x_3^*) \in \mathfrak{S}_{2D}^N$ so that

$$\int_r \int_\theta \operatorname{grad} u^N \operatorname{grad} v^N|_{x_3 = x_3^*} r \, \mathrm{d}r \, \mathrm{d}\theta = \int_r \int_\theta \operatorname{grad} u \operatorname{grad} v^N|_{x_3 = x_3^*} r \, \mathrm{d}r \, \mathrm{d}\theta, \quad \forall v^N(x_3^*) \in \mathfrak{S}_{2D}^N \tag{35}$$

herein grad should be understood as the gradient within the plane perpendicular to the edge at the point x_3^*.

Using Green's theorem (35) becomes

Find $u^N(x_3^*) \in \mathfrak{S}_{2D}^N$ so that

$$\begin{aligned} &\int_\theta \left[u^N \frac{\partial v^N}{\partial r} \right]_{R, x_3^*} R \, \mathrm{d}\theta - \int_r \int_\theta u^N \Delta_{2D} v^N|_{x_3^*} r \, \mathrm{d}r \, \mathrm{d}\theta \\ &\quad = \int_\theta \left[u \frac{\partial v^N}{\partial r} \right]_{R, x_3^*} R \, \mathrm{d}\theta - \int_r \int_\theta u \Delta_{2D} v^N|_{x_3^*} r \, \mathrm{d}r \, \mathrm{d}\theta \quad \forall v^N(x_3^*) \in \mathfrak{S}_{2D}^N \end{aligned} \tag{36}$$

Since $v^N(x_3^*) \in \mathfrak{S}_{2D}^N$ it satisfies identically $\Delta_{2D} v^N = 0$ so that (36) simplifies to

Find $u^N(x_3^*) \in \mathfrak{S}_{2D}^N$ so that

$$\int_\theta \left[u^N \frac{\partial v^N}{\partial r} \right]_{R, x_3^*} R \, \mathrm{d}\theta = \int_\theta \left[u \frac{\partial v^N}{\partial r} \right]_{R, x_3^*} R \, \mathrm{d}\theta \quad \forall v^N(x_3^*) \in \mathfrak{S}_{2D}^N \tag{37}$$

Inserting Equations (12), (14) and (17) into (37), and noting the orthogonality of the eigen-functions $s_i(\theta)$, one obtains after steps similar to these in Section 3:

$$b_i(x_3^*) = a_i(x_3^*) + R^2 c_{i1}(\partial_3^2 a_i(x_3^*)) + R^4 c_{i2}(\partial_3^4 a_i(x_3^*)) + \mathcal{O}(R^6) \tag{38}$$

This equation is very similar to (21) obtained by the L^2 projection method, only that the coefficients multiplying the powers of R^{2i} are somewhat simpler. Therefore, from the theoretical point of view, the application of the energy projection method is expected to provide exactly same behaviour as the L^2 projection method. However, the practical use of the energy projection method is superior to the previous one for the following reason:

- The energy projection method requires integration over a 1-D circular arc, as opposed to 2-D integration required for the L^2 projection method, i.e. a more efficient method.

It is important to note that for a general scalar second order boundary value problem ('anisotropic' heat transfer equation) the conclusions of the aforementioned analysis are similar. The mathematical analysis is more complicated because $\int s_i(\theta)s_j(\theta)\,\mathrm{d}\theta \neq 0$ for $i \neq j$, thus an explicit equation for each b_i cannot be obtained.

The numerical implementation of the energy projection method is along the lines outlined in Section 3.1, so that we provide the final formulation:

$$b_i(x_3^*) = \frac{\alpha_i \displaystyle\int_{\theta=0}^{\omega_{14}} u_{\mathrm{FE}}(R,\theta,x_3^*)s_i(\theta)\,\mathrm{d}\theta}{R^{\alpha_i}\displaystyle\int_{\theta=0}^{\omega_{14}} s_i^2(\theta)\,\mathrm{d}\theta} \tag{39}$$

6. SUMMARY AND CONCLUSIONS

The computation of the stress intensity functions in the neighbourhood of edges in a three-dimensional linear elastic body is of major importance in engineering practice, and some methods for extracting these from finite element solutions have been earlier proposed (see for example Reference [4] and references therein). However, a detailed mathematical framework of the type discussed in the present paper seems not to be available, and the methods are not the most efficient and accurate due to the need of extracting the EFIFs very close to the edge. Towards developing efficient and accurate methods, we consider in this paper the solution of the Laplace equation on 3-D domains in the vicinity of straight edges. This is because both Laplace and elasticity problems are elliptic and therefore their solutions have similar characteristics.

Herein we present the solution in the vicinity of an edge as an asymptotic series involving 2-D eigenpairs with their coefficients called edge flux intensity functions (EFIFs). The eigenvalues are identical to their 2-D counterparts over a plane perpendicular to the edge, however, additional terms are visible in the asymptotic series as compared with the purely 2-D case. Thus, the EFIFs cannot be obtained in a straightforward manner over this two-dimensional plane, and special methods for their computation have to be used. It is important to note that straightforward implementation of 2-D efficient extraction methods for the EFIFs as the contour integral method (also known as the dual singular function method [10]), or the cutoff function method [8], are not possible either, and will lead to false results unless

a proper treatment is incorporated. We present a special method based on L^2 projection and Richardson extrapolation for point-wise extraction of EFIFs from p-finite element solutions. The mathematical analysis is demonstrated by numerical experimentation. A similar but more efficient method, based on 'energy projection', for extracting EFIFs is also proposed.

Understanding the characteristics of 3-D solutions in the neighbourhood of edges for the Laplace equation, and developing efficient methods for the extraction of EFIFs, enables us to extend these methods to elastic domains and compute edge stress intensity functions efficiently.

APPENDIX A

Herein we show that the asymptotic expansion of the solution in the neighbourhood of an edge presented in Section 3 can be brought to the classical expansion of the 3-D solution in terms of Bessel functions. First, we obtain the classical solution, and the point of departure is the Laplace equation in cylindrical coordinates:

$$\frac{1}{r}\frac{\partial}{\partial r}\left(r\frac{\partial u}{\partial r}\right)+\frac{1}{r^2}\frac{\partial^2 u}{\partial \theta^2}+\frac{\partial^2 u}{\partial x_3^2}=0 \tag{A1}$$

By separation of variables, $u(r,\theta,x_3)=R(r)s(\theta)Z(x_3)$, so that (A1) becomes

$$\frac{1}{rR}\frac{\mathrm{d}}{\mathrm{d}r}(rR')+\frac{s''}{r^2 s}+\frac{Z''}{Z}=0 \tag{A2}$$

The last term is independent of r and θ, so it must be a constant denoted by $Z''/Z=\delta$. Multiply by r^2, (A2) becomes

$$\frac{r}{R}\frac{\mathrm{d}}{\mathrm{d}r}(rR')+\frac{s''}{s}+r^2\delta=0 \tag{A3}$$

Again, the second term is θ dependent while other terms are r dependent, so that s''/s has to be a negative constant if oscillatory solution in θ is sought, i.e. $s''/s=-\alpha^2$, thus, $s(\theta)$ is of the form

$$s(\theta)=\mathrm{e}^{\mathrm{i}\alpha\theta} \tag{A4}$$

The values of α are determined by satisfying boundary conditions at $\theta=0$ and ω_{14} — these are the eigenpairs for the 2-D problem, and there is an infinite number of distinct eigenpairs $s_n(\theta)$ which are $\sin(\alpha_n\theta)$ and $\cos(\alpha_n\theta)$.

The case $s''/s=+\alpha^2$ is excluded because it produces a solution which is exponential in θ, thus cannot satisfy boundary conditions. Coming back to (A3):

$$r^2R''+rR'+(\delta r^2-\alpha_n^2)R=0 \tag{A5}$$

there are two possibilities:

$0>\delta=-\gamma^2$:

Define $q=\gamma r$ so that $R(r)=R(q/\gamma)\overset{\text{def}}{=}Q(q)$, and (A5) becomes

$$q^2Q''+qQ'-(q^2+\alpha_n^2)Q=0 \tag{A6}$$

Equation (A6) is the modified Bessel equation and its solution for a domain where $r=0$ is included is the modified Bessel function of first kind of order α_n (see [11, pp. 108–110]):

$$R(r)=I_{\alpha_n}(q)=\sum_{k=0}^{\infty}\frac{(q/2)^{2k+\alpha_n}}{\Gamma(k+1)\Gamma(\alpha_n+k+1)} \tag{A7}$$

where $\Gamma(q)$ is the Gamma function [11, p. 1]:

$$\Gamma(q)\stackrel{\text{def}}{=}\int_0^{\infty}\mathrm{e}^{-t}t^{q-1}\,\mathrm{d}t \tag{A8}$$

Since $Z''/Z=\delta=-\gamma^2$, we immediately obtain an oscillatory behaviour in x_3, and by imposing the boundary conditions at given x_3 we again obtain an infinite number of distinct values of γ_m, i.e. any $Z_m(x_3)$ is given by linear combination of $\sin(\gamma_m x_3)$ and $\cos(\gamma_m x_3)$.

Summarizing, the complete solution u, oscillatory in θ and x_3 is

$$u(r,\theta,x_3)=\sum_{n,m=1}^{\infty}I_{\alpha_n}(\gamma_m r)s_n(\theta)Z_m(x_3) \tag{A9}$$

$0>\delta=+\gamma^2$:

In this case (A5) becomes

$$q^2Q''+qQ'+(q^2-\alpha_n^2)Q=0 \tag{A10}$$

Equation (A10) is the Bessel equation and its solution for a domain where $r=0$ is included is the Bessel function of first kind of order α_n (see [11, p. 102]):

$$J_{\alpha_n}(q)\stackrel{\text{def}}{=}\sum_{k=0}^{\infty}\frac{(-1)^k(q/2)^{2k+\alpha_n}}{\Gamma(k+1)\Gamma(\alpha_n+k+1)} \tag{A11}$$

Since now $Z''/Z=\delta=+\gamma^2$, we immediately obtain an exponential behaviour in x_3: $Z(x_3)=\mathrm{e}^{\pm\gamma x_3}$.

Summarizing, the complete solution u, oscillatory in θ and exponential in x_3 is

$$u(r,\theta,x_3)=\sum_{n=1}^{\infty}J_{\alpha_n}(\gamma r)\mathrm{e}^{\pm\gamma x_3}s_n(\theta) \tag{A12}$$

The value of γ is determined by boundary conditions on $r=constant$. For example, if $u=0$ on $r=C$, then $J_{\alpha_n}(\gamma C)=0$, so that γC is a zero of J_{α_n}.

We now prove that the asymptotic solution presented in Section 3 can be brought to the classical solution (A12) if its behaviour in x_3 is exponential, or to the classical solution (A10) if its behaviour in x_3 is oscillatory. To this end, we first need to introduce the following connections. Integrating by parts (A8) it is easily shown that the Gamma function satisfies the following identity:

$$\Gamma(q+1)=q\Gamma(q) \tag{A13}$$

and by recursive substitution it can be shown that

$$\Gamma(q+k+1) = (q+k)\Gamma(q+k) = (q+k)[(q+k-1)\Gamma(q+k-1)]$$
$$= \cdots = \Gamma(q+1)\prod_{\ell=1}^{k}(q+\ell), \quad k \in \mathbb{N} \tag{A14}$$

Noting that $\Gamma(j) = j!$, for any positive integer j, let us consider the following expression:

$$\Gamma(j+1)\Gamma(q+j+1) = [j\Gamma(j)][(q+j)\Gamma(q+j)]$$
$$= [j(j-1)\Gamma(j-1)][(q+j)(q+j-1)\Gamma(q+j-1]$$
$$= \cdots = \Gamma(q+1)\prod_{k=1}^{j} k(q+k), \quad j \in \mathbb{N} \tag{A15}$$

or writing (A15) in a different form

$$\frac{1}{\prod_{k=1}^{j} k(q+k)} = \frac{\Gamma(q+1)}{\Gamma(j+1)\Gamma(q+j+1)} \tag{A16}$$

Substituting (A16) in the expression (10) of Section 3, the latter becomes

$$S_n(r,\theta,x_3) = r^{\alpha_n} s_n(\theta)\Gamma(\alpha_n+1)\sum_{k=0}^{\infty} \partial_3^{2k} a_n(x_3) r^{2k} \frac{(-0.25)^k}{\Gamma(k+1)\Gamma(\alpha_n+k+1)} \tag{A17}$$

Assume $a_n(x_3)$ has an exponential behaviour in x_3, i.e. it may be represented as follows:

$$a_n(x_3) = \mathrm{e}^{\pm\gamma x_3}, \Rightarrow \partial_3^{2k} a_n(x_3) = \gamma^{2k}\mathrm{e}^{\pm\gamma x_3} \tag{A18}$$

Then after substituting (A18) in (A17) and rearranging, one obtains

$$S_n(r,\theta,x_3) = \frac{2\Gamma(\alpha_n+1)}{\gamma^{\alpha_n}}\,\mathrm{e}^{\pm\gamma x_3} s_n(\theta)\sum_{k=0}^{\infty} \frac{(-1)^k (r\gamma/2)^{2k+\alpha_n}}{\Gamma(k+1)\Gamma(\alpha_n+k+1)} \tag{A19}$$

Note that the definition of the Bessel function of first kind of order α in (A11), $S_n(r,\theta,x_3)$ can be represented in terms of the Bessel function:

$$S_n(r,\theta,x_3) = \frac{2\Gamma(\alpha_n+1)}{\gamma^{\alpha_n}}\,\mathrm{e}^{\pm\gamma x_3} J_{\alpha_n}(\gamma r) s_n(\theta) \tag{A20}$$

Because $[2\Gamma(\alpha_n+1)/\gamma^{\alpha_n}]$ is a constant we can include it in the constant appearing in $s_n(\theta)$, so that (12) in Section 3 is identical to the classical solution (A12).

If instead $a_n(x_3)$ has an oscillatory behaviour in x_3, i.e. it may be represented as follows:

$$a_n(x_3) = \mathrm{e}^{\pm \mathrm{i}\gamma x_3}, \Rightarrow \partial_3^{2k} a_n(x_3) = (-1)^k \gamma^{2k}\mathrm{e}^{\pm \mathrm{i}\gamma x_3} \tag{A21}$$

Then after substituting (A21) in (A17) and rearranging, one obtains

$$S_n(r,\theta,x_3)=\frac{2\Gamma(\alpha_n+1)}{\gamma^{\alpha_n}}\mathrm{e}^{\pm \mathrm{i}\gamma x_3}s_n(\theta)\sum_{k=0}^{\infty}\frac{(r\gamma/2)^{2k+\alpha_n}}{\Gamma(k+1)\Gamma(\alpha_n+k+1)} \tag{A22}$$

Notice the definition of the modified Bessel function of first kind of order α in (A7), $S_n(r,\theta,x_3)$ can be represented in terms of the modified Bessel function:

$$S_n(r,\theta,x_3)=\frac{2\Gamma(\alpha_n+1)}{\gamma^{\alpha_n}}\,\mathrm{e}^{\pm \mathrm{i}\gamma x_3}I_{\alpha_n}(\gamma r)s_n(\theta) \tag{A23}$$

The constant $[2\Gamma(\alpha_n+1)/\alpha_n]$ is included in the constant appearing in $s_n(\theta)$, and $1/\gamma$ is included in the constant of the oscillatory function in x_3, so that (12) in Section 3 is again identical to the classical solution (A9).

REFERENCES

1. Dauge M. *Elliptic boundary value problems in corner domains—smoothness and asymptotics of solutions. Lecture notes in Mathematics*, Vol. 1341. Springer: Heidelberg, 1988.
2. Costabel M, Dauge M. General edge asymptotics of solution of second order elliptic boundary value problems I & II. *Proceedings of the Royal Society of Edinburgh*, Vol. 123A, 1993; 109–184.
3. Babuška I, Von-Petersdorff T, Andersson B. Numerical treatment of vertex singularities and intensity factors for mixed boundary value problems for the Laplace equation in R^3. *SIAM Journal of Numerical Analysis* 1994; **31**(5):1265–1288.
4. Andersson B, Falk U, Babuška I, Von-Petersdorff T. Reliable stress and fracture mechanics analysis of complex components using a h-p version of FEM. *International Journal for Numerical Methods in Engineering* 1995; **38**:2135–2163.
5. Guo B, Oh H-S. The method of auxiliary mapping for the finite element solutions of elliptic partial differential equations on nonsmooth domains in R^3. Preprint submitted for publication to *Mathematics of Computations*, 1996.
6. Grisvard P. *Singularities in boundary value problems*. Masson: France, 1992.
7. Yosibash Z, Szabó BA. Numerical analysis of singularities in two-dimensions. Part 1: Computation of eigenpairs. *International Journal for Numerical Methods in Engineering* 1995; **38**(12):2055–2082.
8. Babuška I, Miller A. The post-processing approach in the finite element method — Part 2: The calculation of stress intensity factors. *International Journal for Numerical Methods in Engineering* 1984; **20**:1111–1129.
9. Yosibash Z. Numerical analysis on singular solutions of the Poisson equation in two-dimensions. *Computational Mechanics* 1997; **20**:320–330.
10. Blum H, Dobrowolski M. On finite element methods for elliptic equations on domains with corners. *Computing* 1982; **28**:53–63.
11. Lebedev NN. *Special Functions and their Applications*. Prentice-Hall: Englewood Cliffs, NJ, 1965.

